

## Dynamical behavior of free electrons in the recombination process in liquid argon, krypton, and xenon

Shinzou Kubota, Masahiko Hishida, Masayo Suzuki, and Jian-zhi Ruan (Gen)

*Rikkyo University, Nisi-Ikebukuro, Tokyo, 171, Japan*

(Received 27 February 1979)

The time dependence of the luminescence due to the recombination process of electrons and ions in liquid argon, krypton, and xenon excited by  $^{207}\text{Bi}$  internal-conversion electrons has been studied by considering the difference curve of two decay curves, the one in the absence of electric field and the one with such a high electric field that all of the observed decay characteristics can be attributed to self-trapped exciton luminescence. The time dependence is well explained by using the kinetic equation for electrons and the recombination process, without diffusion. This provides good evidence for the existence of a strong Coulomb interaction of thermalized electrons and ions. Two excited molecular states  $^1\Sigma_u^+$  and  $^3\Sigma_u^+$  are formed through the recombination process, as in the case of self-trapped exciton luminescence. The recombination cross sections, in units of  $10^{-16} \text{ cm}^2$ , are  $7000 \pm 2000$  for liquid argon,  $120 \pm 30$  for liquid krypton, and  $10 \pm 2$  for liquid xenon. The considerably small values for liquid krypton and xenon compared with that for liquid argon are explained by the unfavorable crossing of the  $R_2^+$  and repulsive  $R_2^{**}$  potential curves in the liquid, based on the theory of dissociative recombination  $R_2^+ + e \rightleftharpoons R_2^{**} \rightarrow R^{**} + R$  in the gaseous state.

### I. INTRODUCTION

Vacuum-ultraviolet luminescence from solid and liquid argon, krypton, and xenon has previously been studied with uv light, x rays, and ionizing charged-particle excitation.<sup>1-6</sup> In all of these investigations, a narrow-band intrinsic luminescence was observed, which was explained as transitions from lowest excited molecular states to the dissociative ground state.

According to experiments by one of the authors<sup>7</sup> (hereafter referred to as I), on the effect of electric fields on the liquid-argon and liquid-xenon luminescence excited by energetic electrons, it was shown that 67% (Ar) and 74% (Xe) of the produced luminescence is due to the excited molecules which are produced through the recombination process of molecular ions  $R_2^+$  and free electrons, and that 33% (Ar) and 26% (Xe) is due to the emission from self-trapped excitons. We call these two types of luminescence, which have the same photon energy, recombination luminescence and self-trapped exciton luminescence.

In a previous paper<sup>8</sup> (hereafter referred to as II), measurements have been reported on the decay curves of the luminescence for liquid argon, krypton, and xenon at such a high field that all of the observed decay characteristics can be attributed to the self-trapped exciton luminescence. An applied electric field quenches the luminescence from free-electron recombination. It has also been shown that self-trapped exciton luminescence has two components, a fast one and a slow one, which correspond

to  $^1\Sigma_u^+ \rightarrow ^1\Sigma_g^+$  and  $^3\Sigma_u^+ \rightarrow ^1\Sigma_g^+$  transitions. In the latter transition, the restriction against multiplicity is removed by the mixing of the  $^3\Sigma_u^+$ -state character with the  $^1\Pi_u$  state due to spin-orbit coupling. Two excited molecular lifetimes,  $\tau_1$  and  $\tau_2$ , for  $^1\Sigma_u^+$  and  $^3\Sigma_u^+$  states, reported in II, are given in Table I.

There exists a considerable literature on the luminescence in rare-gas liquids and solids,<sup>1-6</sup> but little work has been done on the dynamics of recombination luminescence and on the behavior of free electrons in these liquids and solids. In this experiment, we have studied the recombination luminescence in liquid argon, krypton, and xenon excited by  $^{207}\text{Bi}$  internal-conversion electrons. Information about the dynamics of the recombination process associated with free electrons has been derived from the difference curve of the decay curves observed at zero field and at high field.

### II. EXPERIMENTAL PROCEDURE

The experiment consists of decay-curve measurements and the measurement of the luminescence intensities and of the unrecombined charge produced by  $^{207}\text{Bi}$  internal-conversion electrons. The experimental apparatus is similar to that described in I and II and is shown schematically in Fig. 1. A chamber with a glass window and with two electrodes, a cathode and a collector, is used to observe the electric field effect on the luminescence. The cathode is a flat-surface disk with a diameter of 27.5 mm. The collector is an array of wires with a diameter of 10

TABLE I. Two excited molecular lifetimes,  $\tau_1$  and  $\tau_2$ , for  $^1\Sigma_u^+$  and  $^3\Sigma_u^+$  states.

Liquid	$\tau_1$ (ns)	$\tau_2$ (ns)
Argon	$5.0 \pm 0.2$	$860 \pm 30$
Krypton	$2.1 \pm 0.3$	$80 \pm 3$
Xenon	$2.2 \pm 0.3$	$27 \pm 1$

$\mu\text{m}$  strung onto a circular flange with a  $100\text{-}\mu\text{m}$  spacing. The distance between the cathode and the collector is  $5\text{ mm}$ . A  $^{207}\text{Bi}$  internal-conversion electron source (2-mm-diam spot), which emits electrons with energies of 1.05, 0.976, 0.55, and 0.48 MeV, was deposited chemically on the center of the cathode. The radioactive decay rate was about 200 dis/sec.

The inner surface of the glass window is coated with 1,4-*bis* [2-(4-methyl-5-phenyloxazolyl)] benzene (POPOP) to shift the uv luminescence wavelength to the visible region. POPOP itself has a fluorescence decay time of 1.8 ns,<sup>9</sup> and this decay time and the finite resolving time of the apparatus have been allowed for in the analysis of the decay curves as described in II.

A time-to-amplitude converter is started by a trigger pulse from a photomultiplier (RCA 8575) that collects a large fraction of converted luminescence and is stopped by a second photomultiplier (DuMont

56AVP) that collects a much smaller portion of the converted luminescence through a glass fiber. The output from the time-to-amplitude converter is fed into the pulse-height analyzer where the decay curve is accumulated.

To observe the luminescence intensity, the output pulses from the 11th dynode of the photomultiplier (RCA 8575) were clipped through a resistance-capacitance network with a clipping time of about  $1\ \mu\text{s}$ , and then sent through a pulse shaper into the pulse-height analyzer as described in I. In order to ascertain complete charge collection, the collected charge was measured by the pulse technique, also described in I. Signal pulses from the collector were amplified by a charge-sensitive amplifier and a main amplifier with differential and integrating time constants of  $2\ \mu\text{s}$ , and then analyzed by the pulse-height analyzer. Since the differential time constant is larger than the electron drift time (less than  $1\ \mu\text{s}$ ) for field strengths of more than  $3\ \text{kV/cm}$ ,<sup>19</sup> the measured pulse height gives a good measure of the collected charge.

The gas-filling system and the liquifying methods are similar to those described in II.

### III. EXPERIMENTAL RESULTS

The applied electric field produced a decrease in the luminescence intensity as reported in I. Figure 2 shows the curves for the luminescence intensity  $L$  versus the electric field strength  $E$ , together with the saturation curves of the collected charge  $Q$ . The in-

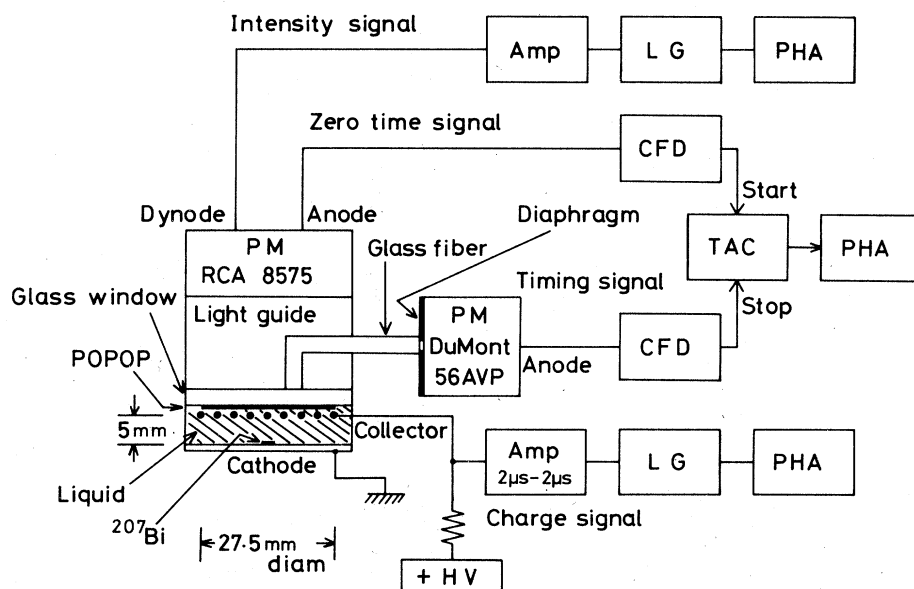


FIG. 1. Block diagram of the electronic system and the chamber used to measure the time dependence of the luminescence intensity. CFD, LG, TAC, and PHA represent a constant-fraction discriminator, a linear-gate circuit, a time-to-amplitude converter, and a pulse-height analyzer.

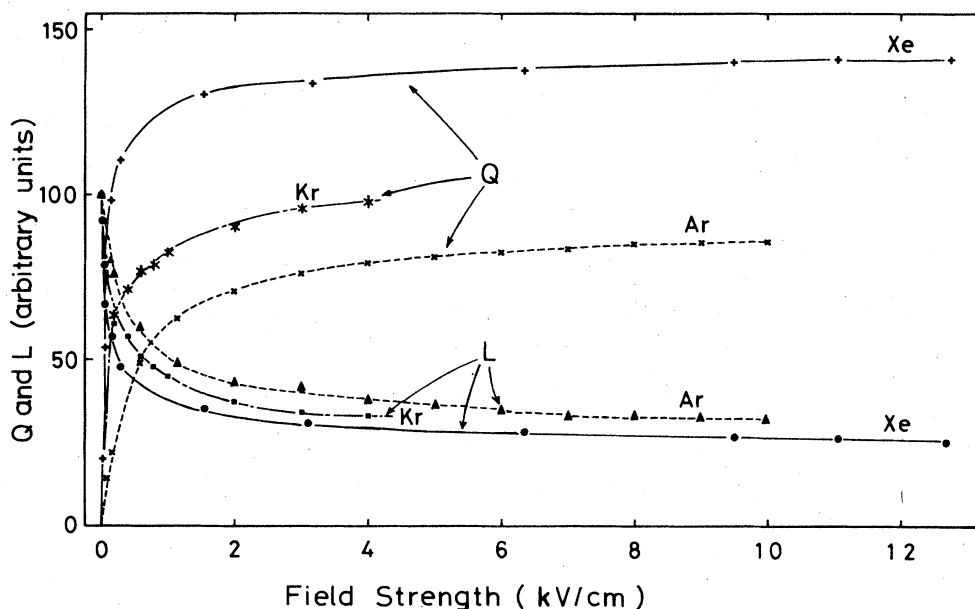


FIG. 2. Variation of relative luminescence intensity  $L$  and collected charge  $Q$  in liquid argon, krypton, and xenon vs applied-electric-field strength for 0.976- and 1.05-MeV electrons.

tensity decreases were 64% at 6 kV/cm for liquid argon and 60 and 70% at 4 kV/cm for liquid krypton and for liquid xenon, respectively, relative to the intensities without an electric field. Reproducible results were obtained for different experimental runs. No photons were detected without POPOP.

Here it is interesting to compare the slopes of the luminescence intensity and collected charge for  $E \leq 3$  kV/cm shown in Fig. 2. The slopes for liquid xenon are steeper than those for liquid argon. This fact suggests that electrons are more easily separated from the positive ions in liquid xenon. This is mainly due to the smaller recombination cross section and partly due to the larger electron mobility in liquid xenon compared with those in liquid argon. A detailed study of the saturation curves will be published elsewhere.<sup>10</sup>

Figure 2 shows that 92% of the produced charge for liquid argon, 94% of that for liquid krypton, and 96% of that for liquid xenon were collected at 4 kV/cm. This confirms that the decay characteristics at such a high field can be attributed to the self-trapped exciton luminescence.

The luminescence intensity can be divided into two constituents  $L_{ex}$  and  $L_r$ , where  $L_{ex}$  is the luminescence intensity due to the self-trapped exciton luminescence and  $L_r$  is due to the recombination luminescence. Under the condition of complete charge collection,  $L_r$  is zero. The values of  $L_r/(L_{ex} + L_r)$  can be obtained from Fig. 2 by the same method as described in I and they are shown in Table II.

Figure 3 shows typical decay curves with and without applied electric fields for liquid argon. They

are plotted so that the ratio of total counts for the two curves are equal to the ratio  $(L_{ex} + L_r)/L_{ex}$ . It can be seen that the decay curve with an applied electric field is similar to the decay curve without an applied electric field. The decay curve for recombination luminescence obtained as the difference of the two decay curves is also shown in Fig. 3. This decay curve shows almost two exponential components and the decay times of the fast and the slow components are 6.3 and 940 ns, respectively.<sup>11</sup> These values are nearly equal to those for self-trapped exciton luminescence (see Table I). This fact suggests that the recombination time is significantly short compared with the decay times for the excited molecular states and that two excited molecular states ( $^1\Sigma_u^+$  and  $^3\Sigma_u^+$ ) are also produced through the recombination of free electrons and positive ions.

Figures 4 and 5 show the decays for the recombination luminescence for liquid krypton and for liquid xenon, respectively, which were obtained by the same method as for liquid argon. As a reference, we

TABLE II. Measured  $L_r/(L_{ex} + L_r)$ , calculated  $R_C$  and  $L$ , and the true range  $R_0$  of 1-MeV electrons.

Liquids	$L_r/(L_{ex} + L_r)$	$R_C(\text{\AA})$	$L(\text{\AA})$	$R_0(\text{cm})$
Argon	0.64	1100	1400	0.58
Krypton	0.67	780	700	0.34
Xenon	0.71	400	440	0.28

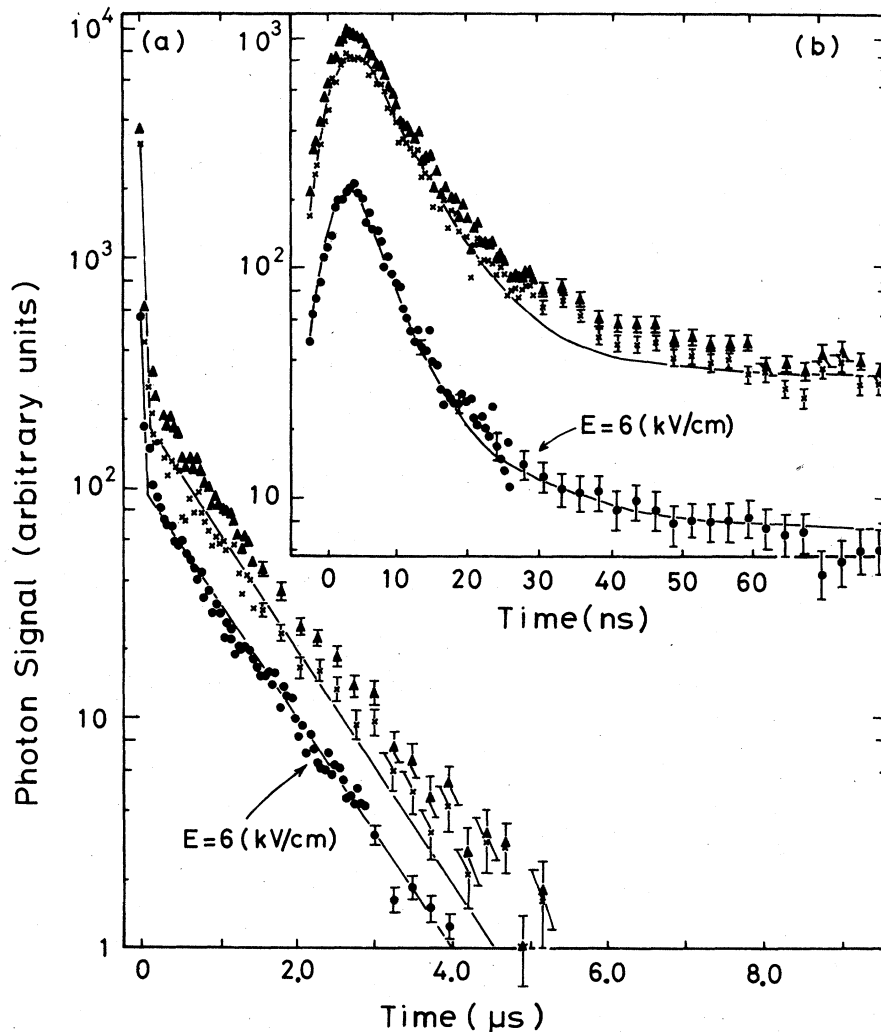


FIG. 3. Time dependence of the luminescence intensity for liquid argon without ( $\blacktriangle$ ) and with ( $\bullet$ ) an applied electric field. The data are plotted so that the total counts for the two curves are equal to the ratio  $(L_{\text{ex}} + L_r)L_{\text{ex}}^{-1}$ . The difference curve ( $\times$ ) of the two decay curves represents the decay curve for the recombination luminescence. The long-time range (a) and the short-time range (b) are indicated. The solid lines represent fitted curves.

also show the decay curves for self-trapped exciton luminescence, in Figs. 4 and 5, which have been reported in II. The decay curves in each figure are plotted so that the total counts for the two curves are equal to the ratio  $L_r/L_{\text{ex}}$ .

In the case of liquid krypton, the two exponential components are not clearly observed in the recombination luminescence, as seen from Fig. 4. The apparent decay time for the time range from 50 to 400 ns is about 88 ns, which is larger than the 80 ns for self-trapped exciton luminescence.

In the case of liquid xenon, a drastic difference is observed between the decays for recombination luminescence and for self-trapped luminescence, as shown in Fig. 5. This suggests that the recombination time is longer compared with the decay times for the excited molecular states.

## IV. DISCUSSION

### A. Physical origin of the luminescence

The two lowest excited molecular states ( $^1\Sigma_u^+$ ,  $^3\Sigma_u^+$ ), responsible for the luminescence of liquid and solid argon, krypton, and xenon excited by charged particles, have two main origins.<sup>12,13</sup> The first one is the direct excitation of exciton states by the primary charged particles and secondary electrons. This excitation process is followed by the self-trapping of free excitons. In this case the two excited molecular states are formed by the self-trapping process within a picosecond,<sup>12</sup> which is too fast to be followed experimentally.

The second origin is the formation of  $^1\Sigma_u^+$  and  $^3\Sigma_u^+$  states through a recombination process between free

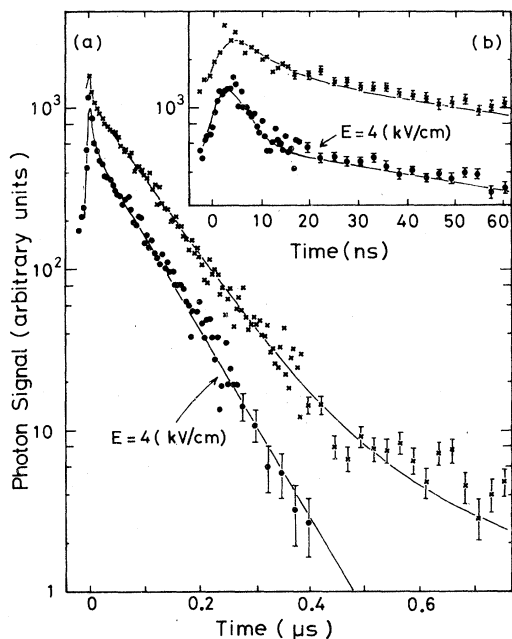


FIG. 4. Time dependences of the recombination luminescence ( $\times$ ) and of the self-trapped exciton luminescence ( $\bullet$ ) for liquid krypton. They are plotted so that the total counts for the two curves are equal to the ratio  $L_r/L_{ex}$ . The long-time range (a) and the short-time range (b) are indicated. The solid lines represent fitted curves.

electrons and molecular ions. The primary particles and secondary electrons produce holes and electrons. The holes are immediately localized through the formation of rare-gas  $R_2^+$  molecular ions within a picosecond,<sup>14-16</sup> while the secondary electrons lose kinetic energy promptly through the excitation of excitons and/or production of electron-hole pairs and then through the emission of phonons. These thermalized electrons finally recombine with localized  $R_2^+$  ions to form the excited molecular states. All these processes are outlined in Fig. 6.

In the study of the time dependence of the luminescence in rare-gas liquids and solids excited by ionizing charged particles, it is therefore necessary to consider two distinct origins of the luminescence. For the first one, called self-trapped exciton luminescence, the decay depends on the excited molecular lifetimes. These excited molecular lifetimes have been studied by applying a high field as described in II.

The second origin, called the recombination luminescence, is attributed to the luminescence from the excited molecular states formed by the recombination process of the molecular ion  $R_2^+$  and the thermalized electrons. The corresponding luminescence has a finite rise time and the time dependence of the luminescence should represent the kinetic characteristics of the recombination process and of the life-

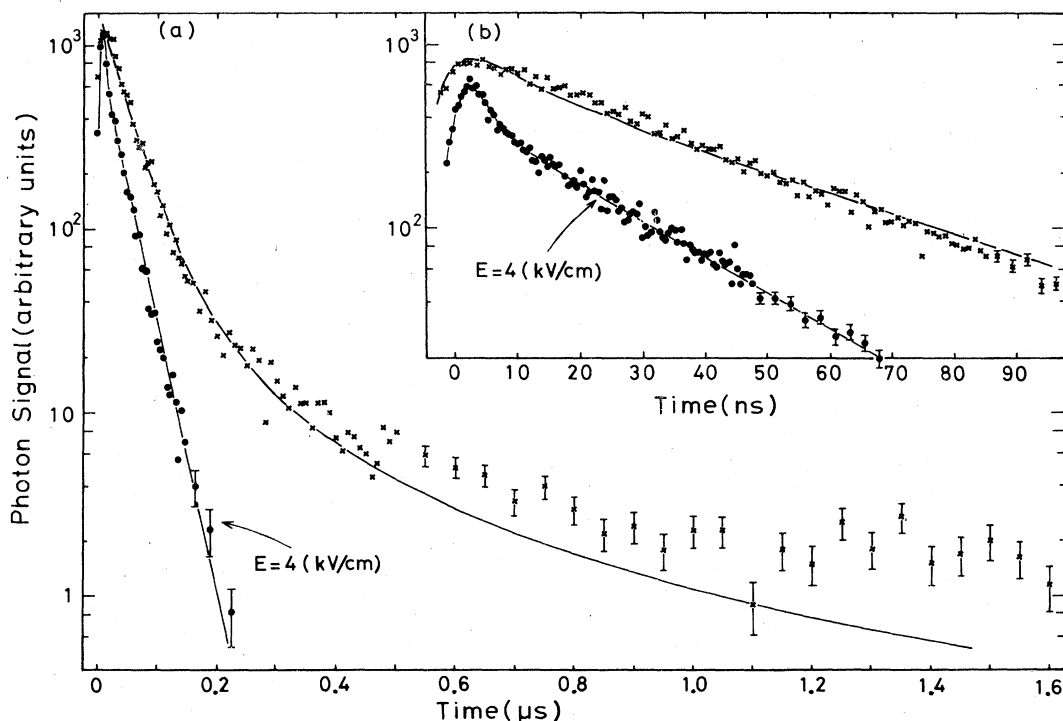


FIG. 5. Time dependences of the recombination luminescence ( $\times$ ) and of the self-trapped exciton luminescence ( $\bullet$ ) for liquid xenon. They are plotted so that the total counts for the two curves are equal to the ratio  $L_r/L_{ex}$ . The long-time range (a) and the short-time range (b) are indicated. The solid lines represent fitted curves.

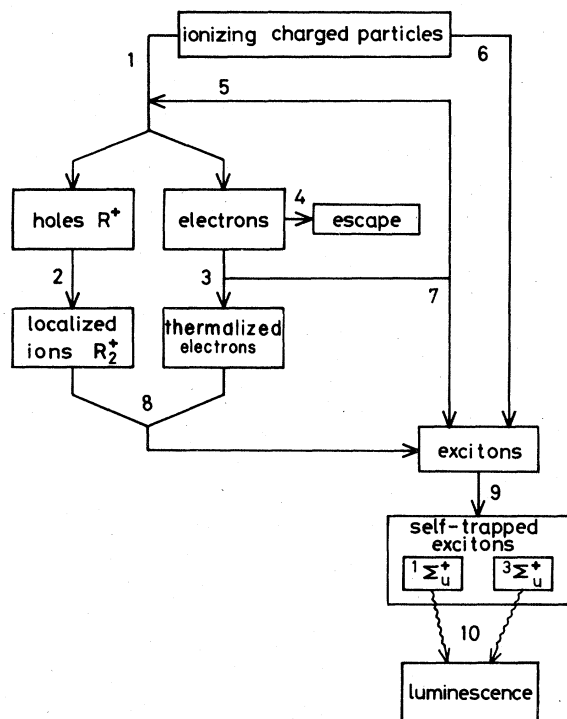


FIG. 6. General reactions occurring in liquid argon, krypton, and xenon excited by ionizing charged particles. 1. Production of electron-hole pairs. 2. Formation of molecular ions,  $R_2^+$ . 3. Thermalization of hot electrons. 4. Escape of hot electrons from the Coulomb attraction of  $R_2^+$  ions. 5. Production of electron-hole pairs by secondary electrons. 6. Production of excitons by the ionizing particle. 7. Production of excitons by secondary electrons. 8. Recombination of free electrons and molecular ions forming excitons. 9. Self-trapping of excitons forming excited molecules. 10. De-excitation of excited molecules emitting uv photons.

times for the two excited molecular states, as shown below.

#### B. Electron kinetics under high-energy-electron excitation

The initial formation of electrons and molecular ions in the case of low specific energy loss can be pic-

tured as follows. The primary energetic electrons leave holes along their tracks and the holes are localized through the formation of  $R_2^+$  molecular ions.<sup>14-16</sup> The average distance  $L$  between neighboring  $R_2^+$  ions is estimated to be 1400, 700, and 400 Å for liquid argon, liquid krypton, and liquid xenon, respectively, for 1-MeV electrons, by using the average energy required to produce one electron-hole pair<sup>17</sup> and the true range  $R_0$  of the primary electron (see Table II).

Following ionization secondary electrons diffuse a distance  $R_d$  determined by the diffusion constant in the presence of the  $R_2^+$ -ion Coulomb attraction and by the thermalization time. Of the electrons produced by ionization, according to the Onsager model,<sup>18</sup> some are trapped in the spheres of Coulomb attraction of their parent ions, some diffuse out of the spheres and are trapped in the spheres of attraction of other ions, and the others escape from the Coulomb attraction. The radius of these spheres is defined as the distance from the positive ion at which the Coulomb energy is equal to the thermal energy:

$$R_C = e^2/\epsilon kT, \quad (1)$$

where  $e$  is the electron charge,  $\epsilon$  is the dielectric constant,  $k$  is Boltzmann's constant, and  $T$  is the absolute temperature. The calculated  $R_C$  values are shown in Table II.

Since the intervals between neighboring  $R_2^+$  ions are expected to be nearly equal and the  $R_C$  value is of the order of  $L$  for the primary energetic electron, we can consider a cylindrical tube of Coulomb attraction with radius  $R_C$  and with length  $R_0$ . In this tube, the Coulomb field is assumed to be uniform from a macroscopic point of view, so the trapped electrons can be considered to be uniformly distributed. Figure 7 shows a schematic illustration of this tube and of the trapped electrons.

In the absence of any diffusion process for the thermalized electrons from the tube, the rate of change of the electron density  $n_-(t)$  is controlled by the coefficient  $\alpha$  of the electron- $R_2^+$ -ion recombina-

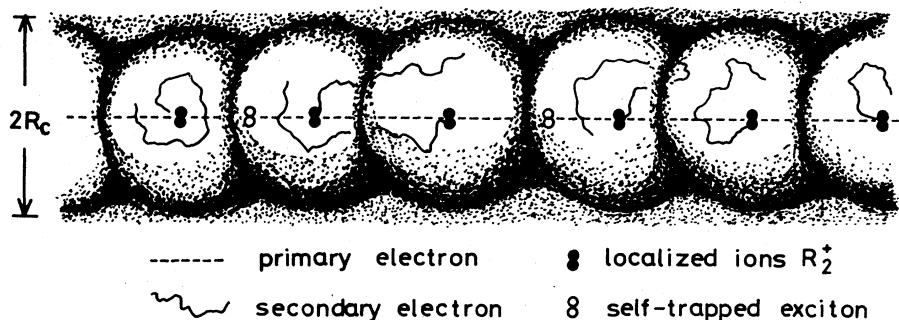


FIG. 7. Illustration of trapped electrons in a cylindrical tube of Coulomb attraction with radius  $R_C$  and length  $R_0$ .

tion according to the equation

$$\frac{dn_-}{dt} = -\alpha n_-(t)n_+(t), \quad (2)$$

under the conditions  $n_-(0) = (1 - \eta)n_0$  and  $n_+(0) = n_0$ . Here,  $\eta$  is the hot-electron escape probability from the tube of Coulomb attraction, and  $n_0$  is the initial number density of electron-hole pairs in the tube and is given by  $N_i/\pi R_C^2 R_0$ , where  $N_i$  is the total number of electron-hole pairs produced by an incident electron. The neglect of the diffusion process has been justified experimentally as discussed below.

The solution of Eq. (2) for  $\eta=0$  is simply

$$n_-(t) = n_+(t) = n_0/(1 + T_r^{-1}t). \quad (3)$$

Here,  $T_r$  is the characteristic recombination time  $(n_0\alpha)^{-1}$ .

### C. Time dependence of the recombination luminescence

We now consider the excited molecules of a state with lifetime  $\tau$  produced by the recombination process. If we denote by  $m(t)$  the number of excited molecules at time  $t$ , its variation is given by

$$\frac{dm(t)}{dt} + \frac{m(t)}{\tau} = \int \alpha n_-(t)n_+(t)dV = f(t). \quad (4)$$

The time dependence  $I(t)$  of the luminescence is given by an equation of the form

$$I(t) \propto \frac{m(t)}{\tau} = \frac{e^{-t/\tau}}{\tau} \int_0^t f(x)e^{x/\tau} dx. \quad (5)$$

In order to have an idea of the general features of  $I(t)$ , we consider two extreme cases. The first case is when the recombination time is short compared with  $\tau$ , so  $f(t)$  is assumed to be a  $\delta$  function. In this case we obtain

$$I(t) \propto \exp(-t/\tau)/\tau. \quad (6)$$

This approximation will hold for liquid argon, since we have obtained two exponential decay components whose decay times are nearly equal to  $\tau_1$  and  $\tau_2$ , as seen from Fig. 3. This fact shows that the recombination time  $T_r$  is much shorter than  $\tau_1$ . As will be shown later,  $T_r$  is found to be  $0.8 \pm 0.2$  ns.

The second case is when  $f(t)$  is a slowly varying function compared with  $e^{-t/\tau}$ . In this case, we have to a good approximation, by using Eq. (2)

$$I(t) \propto f(t)/\tau \quad (7)$$

and

$$I(t) \propto (1 + T_r^{-1}t)^{-2} \quad (7')$$

for  $\eta=0$ . Then a graph of  $I^{-1/2}$  as a function of  $t$  should be linear for  $\eta=0$ . Since Eq. (2) is not easily

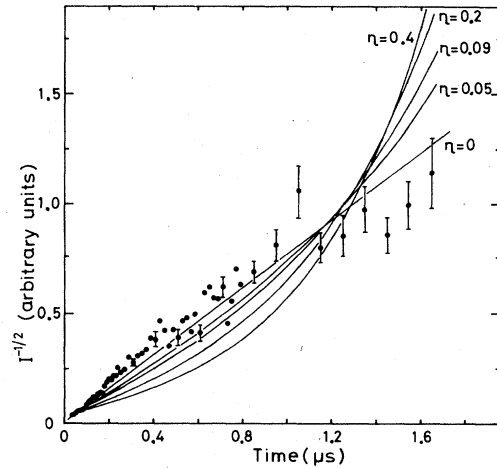


FIG. 8. Variation of  $I^{-1/2}$  with time for liquid xenon. The solid line represents fitted curves for  $\eta=0, 0.05, 0.09, 0.2$ , and  $0.4$ , in which the fitted  $T_r$  values are 10, 25, 40, 65, and 130 ns, respectively.

solved analytically for  $\eta \neq 0$ ,  $n_-(t)$  and  $n_+(t)$  are solved numerically for different  $\eta$  values. The best-fitted curves for  $\eta=0, 0.05, 0.09, 0.2$ , and  $0.3$  are shown in Fig. 8 together with the experimental points for liquid xenon. The  $T_r$  values in these curves are 10, 25, 40, 65, and 130 ns for  $\eta=0, 0.05, 0.09, 0.2$ , and  $0.3$ , respectively. The deviations of the best-fitted curves from the experimental points increase with  $\eta$ . The  $\eta$  value is therefore determined to be less than 0.05. This indicates that the escape probability for hot electrons from Coulomb attraction is very small. Since Eq. (2), in which the diffusion process of the thermalized electrons is neglected, represents the experimental data well, the loss rate of the thermalized electrons by the diffusion process is considered to be negligibly small.

### D. Virtual absence of thermalized-electron diffusion in the presence of positive molecular ions

If there is no interaction between the thermalized electrons and the molecular ions, the electron diffusion length  $(Dt_d)^{1/2}$  in liquid xenon is calculated to be  $5 \times 10^4, 10^5, 5 \times 10^5$  Å for diffusion times  $t_d$  of 10, 35, and 1000 ns, respectively. The diffusion constant  $D$  for electrons without Coulomb attraction of the  $R_2^+$  ion is calculated from the Einstein relation  $D = \mu kT/e$ , where  $\mu$  is the initial electron mobility ( $= 1900 \text{ cm}^2 \text{ s}^{-1} \text{ V}^{-1}$ ) obtained by Miller *et al.*<sup>19</sup> Thus the derived diffusion lengths are appreciably larger than  $R_C$ , which means that the electron kinetic equation (2) should include the diffusion process for the time range of these experimental conditions. However, the experimental results show that this is not the case. This strongly indicates that the Coulomb interaction between the thermalized elec-

trons and molecular ions is strong enough to prevent electron diffusion.

#### E. Relative importance of singlet and triplet excited molecular states in recombination luminescence

In the above discussion we simply assumed that the excited molecules with lifetime  $\tau$  are produced by the recombination process. However, Fig. 3 shows that the singlet molecular states as well as the triplet molecular states are formed through a recombination process. By taking into account two types of excited molecular states with lifetimes  $\tau_1$  and  $\tau_2$ , the form of the time dependence of the recombination luminescence is then

$$I(t) = A_1 I_1(t) + A_2 I_2(t) \quad (8)$$

where  $I_1(t)$  and  $I_2(t)$  are given by Eq. (5) with  $\tau$  replaced by  $\tau_1$  and  $\tau_2$ , respectively, and are normalized as unity. Here,  $A_1$  and  $A_2$  are relative photon numbers.

By using the values of  $\tau_1$  and  $\tau_2$  shown in Table I, the values of  $T_r$  and  $A_1/A_2$  best fitted to the experimental decay curves were evaluated; the values obtained are shown in Table III. The standard deviation of the Gaussian apparatus function of 2.0 ns and a fluorescence decay time of 1.8 ns for the wavelength shifter have been allowed for in the fitting, as described in II. Figure 9 shows the fitted decay curves  $A_1 I_1(t)$ ,  $A_2 I_2(t)$ , and  $I(t)$  for the short-time range. A detailed calculation and its result have been reported by Hishida *et al.*<sup>20</sup> The fitted decay curves  $I(t)$  are also shown in Figs. 3–5.

The ratio  $A_{\text{ex1}}/A_{\text{ex2}}$  of the photon number for the  $^1\Sigma_u^+$  state to that for the  $^3\Sigma_u^+$  state for the self-trapped-exciton luminescence in Figs. 3–5 is also shown in Table III. If the relaxation mechanism producing the  $^1\Sigma_u^+$  and  $^3\Sigma_u^+$  states involved in the recombination-luminescence process is the same as that for the self-trapped-exciton luminescence process, then the value  $A_1/A_2$  must be of the same order as  $A_{\text{ex1}}/A_{\text{ex2}}$ . As seen from Table III, however,

TABLE III. Fitted values  $T_r$  and  $A_1/A_2$  for recombination luminescence and  $A_{\text{ex1}}/A_{\text{ex2}}$  for self-trapped exciton luminescence.

Liquid	$T_r$ (ns)	$A_1/A_2$	$A_{\text{ex1}}/A_{\text{ex2}}$
Argon	$0.8 \pm 0.2$	$0.5 \pm 0.2^a$	$0.36 \pm 0.06$
Krypton	$10 \pm 2$	$0.3 \pm 0.1$	$0.11 \pm 0.02$
Xenon	$15 \pm 2$	$0.8 \pm 0.2$	$0.17 \pm 0.05$

<sup>a</sup>See Ref. 29.

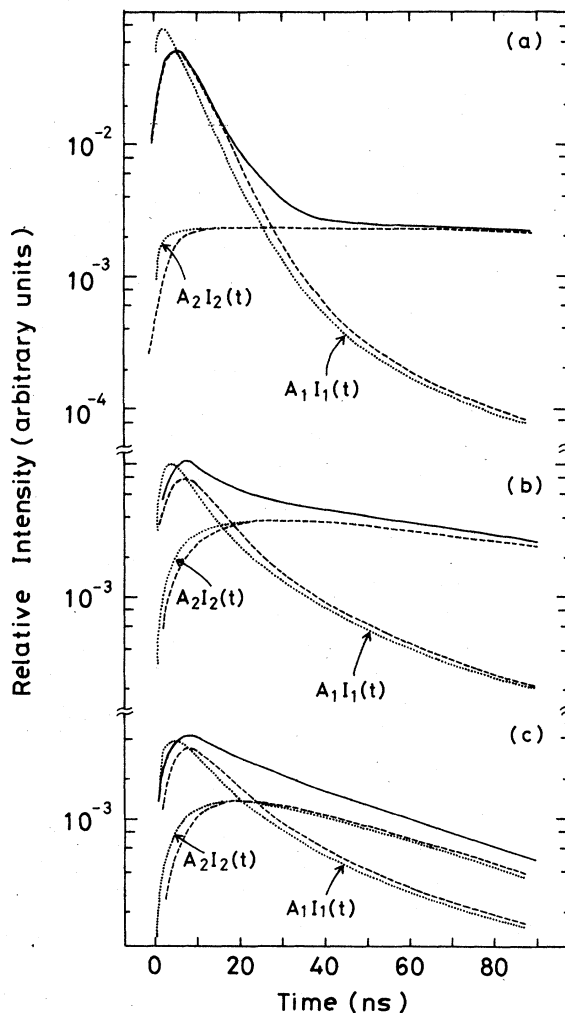


FIG. 9. Solid lines are the curves best fitted to the experimental recombination-luminescence points in the short-time range for liquid argon (a), liquid krypton (b), and liquid xenon (c). The experimental points are shown in Figs. 3(b)–5(b). The dotted lines show the calculated  $A_2 I_1(t)$  and  $A_2 I_2(t)$ . The dashed lines show  $A_1 I_1(t)$  and  $A_2 I_2(t)$  including the 1.8-ns decay time of POPOP and the 2-ns resolving time of the apparatus.

$A_1/A_2$  is two to five times larger than  $A_{\text{ex1}}/A_{\text{ex2}}$  for liquid krypton and liquid xenon, indicating that the relaxation mechanism for the recombination-luminescence process is not the same as that for the self-trapped-exciton luminescence process for these two liquids.

#### F. Recombination process in liquid argon, krypton, and xenon

The cross section for electron- $R_2^+$  recombination can be found from the measured  $T_r$  values and from the equation  $\sigma = (n_0 T_r v)^{-1}$ , where  $v = (3kT/m^*)^{1/2}$  is

TABLE IV. Measured  $\sigma$  and comparison of the dissociative recombination cross section  $\sigma_{\text{gas}}$  in the gaseous state for the electron temperature  $T$  of corresponding liquid. Effective electron mass  $m^*$  in units of the electron mass  $m$ , and electron velocity  $v$  in the liquid.

Liquid	$\sigma$ ( $10^{-16}$ cm $^2$ )	$\sigma_{\text{gas}}$ ( $10^{-16}$ cm $^2$ )	$T$ (K)	$m^*/m$	$v$ ( $10^7$ cm)
Argon	$7000 \pm 2000$	$2000^a$	90	$0.49^b$	0.9
Krypton	$120 \pm 30$	$3000^a$	120	$0.42^b$	1.1
Xenon	$10 \pm 2$	$2000^a$	183	$0.3^b$	1.7

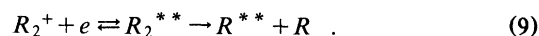
<sup>a</sup>Reference 21.

<sup>b</sup>G. Baldini, Phys. Rev. **128**, 1562 (1962).

the velocity of electrons under thermal equilibrium at the liquid temperature  $T$ . The values of  $\sigma$  so obtained, together with the values of  $v$  and  $m^*$ , are shown in Table IV. The  $\sigma$  values for liquid argon are considerably larger than those for liquid krypton and liquid xenon. The table also shows the recombination cross sections in the gas phase. It can be concluded that with our model the recombination cross section in liquid argon is larger than that in the gas phase. It is certain that the cross sections for liquid krypton and xenon are considerably smaller than those for the gaseous state.

In the gaseous state, the recombination of a molecular ion  $R_2^+$  and an electron is considered to be a dissociative process, which is represented by the

reaction<sup>21</sup>



In a collision of an electron with a molecular ion  $R_2^+$  an intermediate state of the neutral molecule  $R_2^{**}$  is formed. This state is unstable, since an electron can be re-emitted through autoionization. If dissociation of the state  $R_2^{**}$  is possible, however, two neutral atoms can be formed, often in an excited state  $R^{**}$ .

For dissociative recombination of thermal electrons it is necessary that the potential-energy curves for  $R_2^{**}$  come close to that of the ion  $R_2^+$  and preferably cross it within the range of the nuclear vibra-

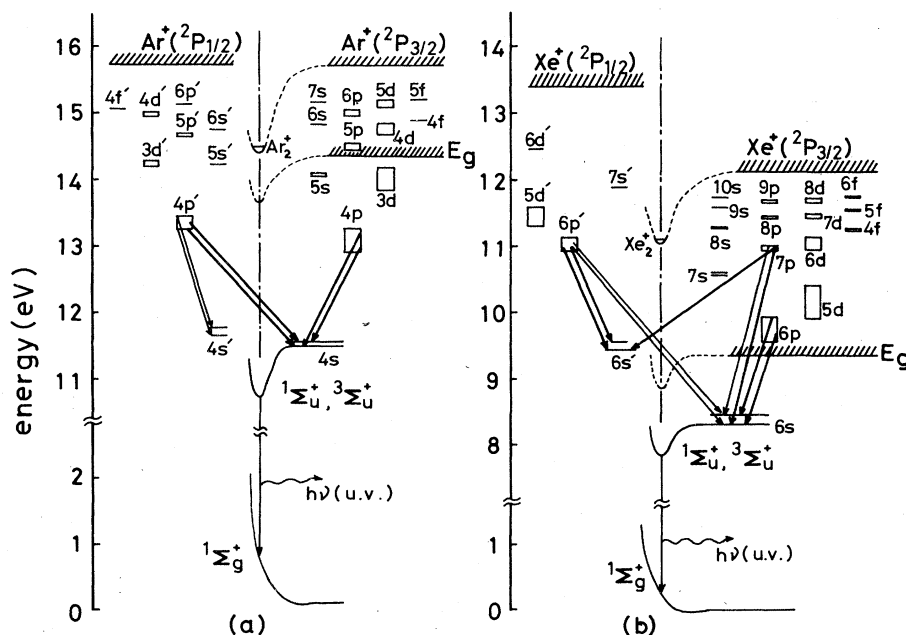


FIG. 10. Partial energy-level diagram for argon (a) and for xenon (b) showing typical observed transitions resulting from dissociative recombination of  $\text{Ar}_2^+$  or  $\text{Xe}_2^+$  ions and electrons in the gaseous state, cited from Refs. 22 and 23. The estimated  $\text{Ar}_2^+$  and  $\text{Xe}_2^+$  potential-energy curves for liquid argon and for liquid xenon are also shown. See Ref. 24.

tions. It has been considered that the potential curves of  $R_2^+$  and  $R_2^{**}$  do cross in the cases of argon, krypton, and xenon.<sup>21</sup>

In the gaseous state, the excited states that are produced by dissociative recombination are found by an optical method due to Shiu and Biondi.<sup>22,23</sup> Their results show that the  $(n+1)p$  and  $(n+1)p'$  states are the most strongly populated, where  $n$  is 3, 4, and 5 for argon, krypton, and xenon, respectively. Figure 10 illustrates partial energy diagrams showing representative transitions observed in experiments on dissociative recombination cited from Ref. 22 and 23.

By extending the above considerations to the liquid state, the probable explanation of the small cross sections for liquid xenon and for liquid krypton is that there is no favorable crossing between  $Xe_2^+$  ( $Kr_2^+$ ) and the repulsive  $Xe_2^{**}$  ( $Kr_2^{**}$ ) potential curves. Although potential-energy curves in the liquid state are not available at present, an estimate may be made approximately by lowering the  $R_2^+$  potential-energy curve from  $I_p$  to  $E_g$ , where  $I_p$  and  $E_g$  are the ionization potential of atom  $R$  and the band-gap energy.<sup>24</sup> Thus, estimated  $R_2^+$  potential-energy curves for liquid argon and for liquid xenon are also shown in Fig. 10. As seen from the figure, for the case of liquid xenon the  $(n+1)p$  and  $(n+1)p'$  states ( $n=5$ ) are embedded in the continuum. On the contrary, these states are most strongly populated in the gaseous state. In the case of liquid argon these states ( $n=3$ ) are not embedded in the continuum. Thus it is expected that there are only a few favorable dissociative states in liquid xenon and krypton,<sup>25</sup> but there are many in liquid argon.

It has been implicitly assumed in the above arguments that the thermalization time of the electrons is too fast compared with the recombination time. Davis and Pai<sup>26</sup> have reported that the rate of energy loss by phonon emission is independent of the excess energy of hot electrons and is given by  $h\nu_p^2$ , where  $h$  is Planck's constant and  $\nu_p$  is a characteristic phonon frequency. By using the Debye frequency<sup>27</sup> for  $\nu_p$  the typical thermalization times are calculated to be 0.9, 1.3, and 1.5 ns at the electron energy of  $\frac{1}{2}E_1$  for liquid argon, krypton, and xenon, respectively, where  $E_1$  is the first-exciton energy. Since the value obtained for liquid argon is of the same order as  $T_r$ , this fact must be considered in electron kinetics. Further investigations, including hot-electron kinetics, are

needed to obtain information concerning the thermalization of hot electrons in rare-gas liquids.

Finally, it is worth noting that the cross section  $\sigma$ , which we have measured in this experiment, gives the magnitude of the region where the electrons recombine with positive ions. Evidently this cross section is not the same as the Coulomb capture cross section,  $\sim R_C^2$ , which is measured by the rate at which electrons leave the conduction band. After the electrons are captured in the Coulomb attraction, the electron-recombination process is determined by the  $\sigma$  value. This was already pointed out in the paper by Lax on cascade capture in semiconductors,<sup>28</sup> but it is not well understood from the experimental point of view.

## V. CONCLUSIONS

From experiments on luminescence in liquid argon, krypton, and xenon excited by energetic electrons, the following conclusions were drawn: (i) Two excited molecular states  $^1\Sigma_u^+$  and  $^3\Sigma_u^+$  are formed through the recombination process of free electrons and molecular ions. (ii) The time dependence of the recombination luminescence is governed by the decay rates of two excited molecular states in liquid argon and by the recombination rate in liquid xenon. (iii) The recombination cross sections show a large variation and decrease in going from argon to krypton to xenon. The cross sections for liquid krypton and xenon are considerably smaller than that for liquid argon. This is explained by the unfavorable crossing of the  $Kr_2^+$  ( $Xe_2^+$ ) and repulsive  $Kr_2^{**}$  ( $Xe_2^{**}$ ) potential curves. (iv) The Coulomb interactions between thermalized electrons and molecular ions are strong.

## ACKNOWLEDGMENTS

The authors wish to thank Professor T. Doke and Dr. T. Takahashi for valuable discussions on the electrons distribution in rare-gas liquids, and wish to thank Professor U. Toyozawa and Professor K. Takayanagi for stimulating discussions on the recombination process. They are much indebted to Professor E. Tajima for encouragement throughout this work. They are also grateful to Dr. T. A. King for reading the manuscript and for his critical comments. The computer fittings were performed at the Rikkyo University Computer Center.

<sup>1</sup>J. Jortner, L. Meyer, S. A. Rice and E. G. Wilson, J. Chem. Phys. **42**, 4250 (1965).

<sup>2</sup>T. Nanba, N. Nagasawa, and M. Ueta, J. Phys. Soc. Jpn. **37**, 1031 (1974).

<sup>3</sup>T. Chesnovsky, B. Raz, and J. Jortner, J. Chem. Phys. **57**, 4628 (1972).

<sup>4</sup>A. Gedanken, B. Raz, and J. Jortner, J. Chem. Phys. **59**, 5471 (1973).

<sup>5</sup>E. E. Koch, C. Kunz, and B. Sonntag, Phys. Rep. **29**, 153 (1977).

<sup>6</sup>I. Ya. Fugol', Adv. Phys. **27**, 1 (1978).

<sup>7</sup>S. Kubota, A. Nakamoto, T. Takahashi, E. Shibamura, M.

- Miyajima, K. Masuda, and T. Doke, *Phys. Rev.* **17**, 2762 (1978).
- <sup>8</sup>S. Kubota, M. Hishida, and J. Ruan(Gen), *J. Phys. C* **11**, 2645 (1978).
- <sup>9</sup>J. B. Birks, *Photophysics of Aromatic Molecules* (Wiley, London, 1970), p. 124.
- <sup>10</sup>T. Takahashi and T. Doke, (unpublished).
- <sup>11</sup>In addition to the fast (6.3 ns) and slow (940 ns) components a 40–180-ns decay component (about 15% of the total photons) is observed in the recombination luminescence of liquid argon. The origin of this component is unknown at present. See Ref. 20.
- <sup>12</sup>M. Martin, *J. Chem. Phys.* **54**, 3289 (1971).
- <sup>13</sup>A. G. Molchanov, *Sov. Phys. Usp.* **15**, 124 (1972).
- <sup>14</sup>K. S. Song, *Can. J. Phys.* **49**, 26 (1971).
- <sup>15</sup>S. D. Druger and R. S. Knox, *J. Chem. Phys.* **50**, 3143 (1969).
- <sup>16</sup>P. G. LeComber, R. J. Loveland, and W. E. Spear, *Phys. Rev. B* **11**, 3124 (1975).
- <sup>17</sup>T. Takahashi, S. Konno, T. Hamada, M. Miyajima, S. Kubota, A. Nakamoto, A. Hitachi, E. Shibamura, and T. Doke, *Phys. Rev. A* **12**, 1771 (1975).
- <sup>18</sup>I. Onsager, *Phys. Rev.* **54**, 554 (1938).
- <sup>19</sup>L. S. Miller, S. Howe and W. E. Spear, *Phys. Rev.* **166**, 871 (1968).
- <sup>20</sup>M. Hishida, M. Suzuki, J. Ruan(Gen), and S. Kubota. See AIP document no. PAPS PRBMDO-20-3486-19 for 19 pages of detailed original calculation for paper "Dynamical behavior of free-electrons...." Order by PAPS number and journal reference from American Institute of Physics, Physics Auxiliary Publication Service, 335 East 45th Street, New York, N. Y. 10017. The price is \$1.50 for each microfiche (98 pages), or \$5 for photocopies of up to 30 pages. Airmail additional. Make checks payable to the American Institute of Physics. This material also appears in *Current Physics Microform*, the monthly microfilm edition of the complete set of journals published by AIP, on the frames immediately following this journal article.
- <sup>21</sup>J. N. Bardsley and M. A. Biondi, *Advances in Atomic and Molecular Physics* (Academic, New York, 1970), Vol. 6, p. 1.
- <sup>22</sup>J.-Y. Shiu and M. A. Biondi, *Phys. Rev. A* **17**, 868 (1978); **A** **16**, 1817 (1977).
- <sup>23</sup>J.-Y. Shiu, M. A. Biondi, and D. P. Sipler, *Phys. Rev.* **15**, 494 (1977).
- <sup>24</sup>We assumed that (i) the electronic band structures of the liquids are almost the same as those of the solids and (ii) the electronic potential curves for the two lowest excited states  $^1\Sigma_u^+$  and  $^3\Sigma_u^+$  in the liquids are the same as those in the solid and gaseous states. The validity of assumption (i) has been experimentally supported by the observation of exciton-enhanced ionization for xenon dopant in liquid argon. [S. Kubota *et al.*, *Phys. Rev. B* **13**, 1649 (1976).] The assumption (ii) has been experimentally supported by the fact that the luminescence spectra in liquids are almost the same as those in solids or gaseous states. The binding-energy values for  $\text{Ar}_2^+$  and  $\text{Xe}_2^+$  ions in liquids are taken from Ref. 14.
- <sup>25</sup>For the case of liquid krypton,  $(n+1)p$  and  $(n+1)p'$  states ( $n=4$ ) are also embedded in the continuum. This is analogous to the situation in liquid xenon as in Fig. 10.
- <sup>26</sup>D. M. Pai and R. C. Enck, *Phys. Rev.* **11**, 5163 (1975).
- <sup>27</sup>M. K. Klein and J. A. Venables, *Rare Gas Solids* (Academic, New York, 1976), Vol. 1, pp. 30, 245, and 250.
- <sup>28</sup>M. Lax, *Phys. Rev.* **119**, 1502 (1960).
- <sup>29</sup>Corrected for the 40–180-ns decay component (see Ref. 20). The fitted  $A_1/A_2$  values for Figs. 3(a) and (b) are 0.9 and 0.37, respectively. This large difference in fitted values is due to the contribution for the 40–180-ns component. This component is regarded, in the fitting, as a slow component in the short-time range [Fig. 3 (b)] or as a fast one in the long-time range [Fig. 3 (a)].